ACS OMEGA

http://pubs.acs.org/journal/acsodf

Article

Venlafaxine Caffeic Acid Salt: Synthesis, Structural Characterization, and Hypoglycemic Effect Analysis

Hongmei Yu, Yong Zhang, Cheng Xing, Ying Wang, Hailu Zhang, Ningbo Gong,* Yang Lu,* and Guanhua Du

Cite This: *ACS Omega* 2021, 6, 13895−13903

Read Online

ACCESS | Metrics & More | Article Recommendations | Supporting Information

ABSTRACT: Depression is a recurrent and chronic mental disorder requiring long-term treatment. Major depressive disorder is present in 15−20% of patients with type 1 or type 2 diabetes. Large-scale evidence revealed that depression and depressive symptoms are independent risk factors for the development of type 2 diabetes, and they may contribute to hyperglycemia and even accelerate the premature onset of diabetes complications. Venlafaxine is a clinical first-line antidepressant used for more than 30 years. Recently, clinical reports showed that venlafaxine overdose might cause hypoglycemia. Venlafaxine is insoluble and salt formation technology is the most appropriate method to improve the physicochemical properties and the pharmacokinetic profile of the drug. In the present work, the use of the solvent evaporation method, slurry, and the liquid-assisted grinding method resulted in the crystalline salt venlafaxine−caffeic acid (1:1). The compounds were characterized using a series of solid-state techniques, viz., powder X-ray diffraction, differential scanning calorimetry, thermogravimetric analysis, Fourier transform infrared spectroscopy, and solid-state nuclear magnetic resonance, and the crystal structure was determined by single-crystal X-ray diffraction. Besides, a comparative study of solubility, dissolution, and hypoglycemic activity of the parent drug and the new salt has been carried out. The tested venlafaxine−caffeic acid salt showed about 16-fold higher solubility than the pure drug. Moreover, the glucose consumption assay results showed that the novel salt possesses potent hypoglycemic activity *in vitro*, suggesting that it is a promising candidate effective for major depressive disorder patients with type 2 diabetes.

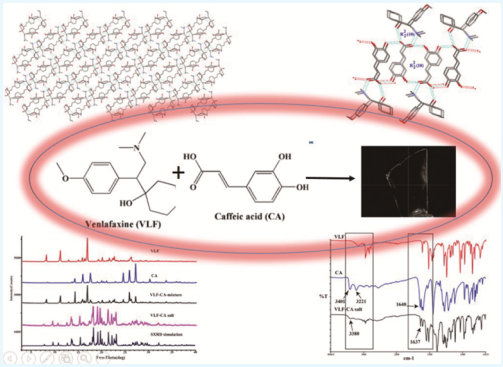

1. INTRODUCTION

Venlafaxine {IUPAC Name:1-[2-(dimethylamino)-1-(4-methoxyphenyl)-ethyl] cyclohexanol, Figure 1, Molecular formula: $C_{17}H_{27}NO_2$, VLF}, an important serotonin-norepinephrine reuptake inhibitor,[1] is being used as a first-line antidepressant since 1993.[2] Venlafaxine was proved effective and safe in the treatment of major depressive disorder,[3] fibromyalgia,[4] postpartum major depression,[5] obsessive-compulsive disorder,[6] generalized anxiety disorder,[7] neuropathic pain,[8,9] attention-deficit/hyperactivity disorder,[10] and diabetic neuropathy.[11] VLF is as effective as other available antidepressants with fewer adverse drug reactions like anticholinergic and cardiotoxicity.[12]

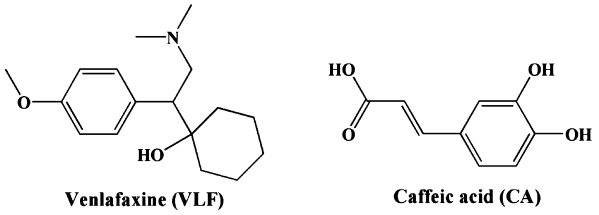

Figure 1. Molecular diagram of venlafaxine (VLF) and caffeic acid (CA).

No less than six polymorphs of venlafaxine hydrochloride have been reported,[13−15] including single X-ray structures of two polymorphs (forms 1 and 2), melt (form 3), hydrate (form 4), sublimation (form 5), and a more stable polymorph (form 6) obtained by the solid-to-solid phase transition of forms 1 or 2. Venlafaxine hydrochloride is marketed in forms 1 and 2 or their mixture with form 6. Over the last three decades, crystal engineering has received widespread attention in the pharmaceutical industry, and various approaches including salt formation and cocrystallization techniques have been followed to modify the physicochemical properties and the pharmacokinetic profiles of VLF. Two inorganic acid salts (hydrochloride[16] and hydrobromide[17]) and thirteen organic acid salts (benzenesulfonic acid, saccharin, coumaric, ferulic,

Received: March 24, 2021
Accepted: May 4, 2021
Published: May 17, 2021

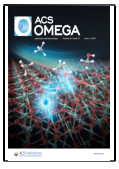

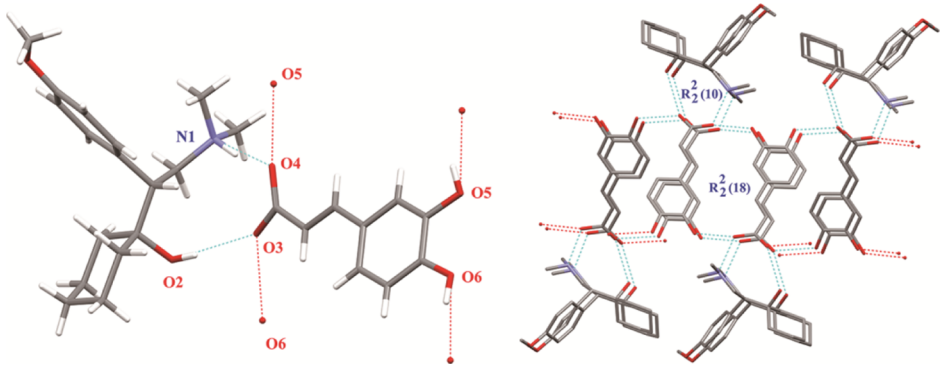

Figure 2. Crystal structure and the 1D and 2D salt bonds and H-bond contacts of VLF−CA.

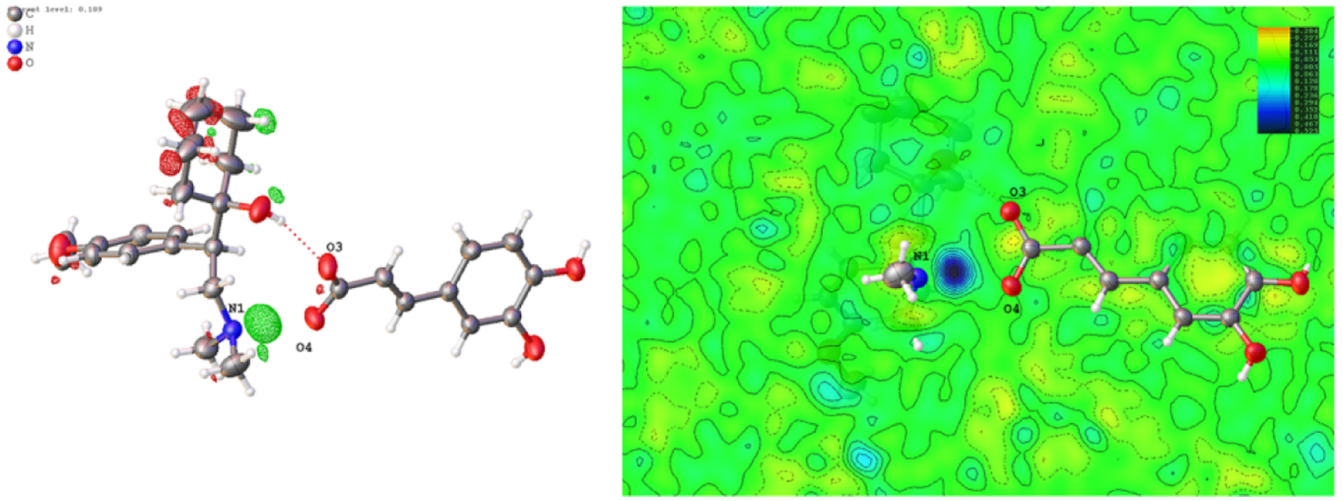

Figure 3. Residual density map for VLF−CA.

oxalic, salicylic, fumaric, citric acid, maleic acid, phthalic acid, 4-chlorobenzene acid, 4-hydroxybenzoic acid, and sulfanilic acid),[18,19] and one cocrystal (celecoxib−venlafaxine)[20] were obtained.

It is estimated that in 2020, chronic diseases will be responsible for the majority of deaths and disabilities worldwide.[21] Both depression and diabetes are debilitating chronic diseases that are associated with the deterioration of health, high healthcare costs, significant morbidity, risk factors for cardiovascular diseases, and even mortality.[22] Considerable evidence indicates that patients with major depressive disorders, a relatively common and costly central nervous system syndrome, are more likely to have poorer health outcomes including uncontrolled blood sugar, complications from diabetes, and higher rates of all-cause mortality.[23−25] During the past few decades, large-scale studies examining the relationship between depression and diabetes revealed that not only are antecedent depression and depressive symptoms independent risk factors for the development of type 2 diabetes but they have also been shown to contribute to hyperglycemia, functional disability among diabetic patients, and may accelerate the premature onset of diabetes complications.[26−31] A meta-analysis conducted by Mezuk et al.[32] explored the hypothesis of bidirectionality between depression and diabetes and documented an increased prevalence of depression among diabetic populations, and conversely, depression serves as a risk factor for the development of diabetes.[33,34] On the other hand, there are clinical reports that show venlafaxine intoxication was frequently followed by severe hypoglycemia.[35,36] Though further studies are necessary to establish a causal relationship between comorbid diabetes distress and depression disorders, the literature illuminated the idea of developing novel candidates that are effective for patients with major depression disorder and diabetes, from which, our research efforts of finding a new venlafaxine salt were encouraged.

In the present work, we present the development of a new salt of venlafaxine with caffeic acid (VLF−CA) which shows a moderate improvement in the physicochemical properties as compared to the pure drug. The crystal arrangements and molecular interactions of the obtained salt were analyzed by single-crystal X-ray diffraction (SXRD) technology. Moreover, the salt was characterized by the application of multi-analytical techniques, powder X-ray diffraction (PXRD), differential scanning calorimetry (DSC), thermogravimetric analysis (TGA), Fourier transform-infrared (FT-IR) spectroscopy, and solid-state nuclear magnetic resonance (ssNMR) measurements. The comparative solubility, stability, and hypoglycemic effect experiments were also performed, with the salt showing a moderate improvement in the physicochemical properties. Pleasantly, the glucose consumption assay results showed that VLF−CA possessed potent hypoglycemic activity *in vitro*, suggesting that it is a prospective candidate that is effective for treating depression with type 2 diabetes.

https://doi.org/10.1021/acsomega.1c01581
ACS Omega 2021, 6, 13895−13903

Table 1. Salt Bond and Hydrogen Bond Geometries for VLF−CA

sample	D-H···A	d(D···A) (Å)	∠(DHA) (deg)	symmetry code
VLF-CA	$N_1-H_1\cdots O_4$	2.795	162.70	$[x, y, z-1]$
	$O_2-H_{2A}\cdots O_3$	2.847	160.45	$[x, y, z-1]$
	$O_5-H_{5A}\cdots O_4$	2.726	146.86	$[-x+2, -y+1, -z+2]$
	$O_6-H_{6A}\cdots O_3$	2.656	165.77	$[-x+3/2, y-1/2, -z+3/2]$

2. RESULTS AND DISCUSSION

2.1. Crystal Structure of VLF−CA Salt. The crystal packing diagram is shown in Figure 2, and the whole molecular network is infinitely extended along the [101] direction. The VLF−CA salt crystallized in the $P2_1/n$ space group with one VLF molecule and one CA molecule in the asymmetric unit. The SXRD data suggested that the N−H proton transferred from CA to VLF, as is shown in the residual density map (Figure 3). An ORTEP-type view of the asymmetric unit with a 50% probability ellipsoid is shown in Figure S3. The distances of C═O and C−OH within the carboxyl group in the CA differ by less than 0.03 Å (0.002 Å), which also proves that the VLF−CA should be considered as a salt.[37] The $N-H^+$ and COO^- ions are bonded through the ionic bond $N_1-H_1\cdots O_4$ (d: 2.795 Å, θ: 162.70°). The ionic bond and intermolecular hydrogen bonds $O_2-H_{2A}\cdots O_3$ (d: 2.847 Å, θ: 160.45°) form a ring. Two neighboring CA motifs form a ring via $O_5-H_{5A}\cdots O_4$ (d: 2.726 Å, θ: 146.86°) hydrogen bond with a head to tail contact, and the next neighboring CA motifs form a clockwise helix along the [010] direction via $O_6-H_{6A}\cdots O_3$ (d: 2.656 Å, θ: 165.77°) hydrogen bond.

The salt bond and hydrogen bond geometrical parameters are given in Table 1. The final data collection parameters and refinement statistics for the structures are summarized in Table 2. The CIF for each refinement and the check CIF files for VLF−CA are available in the Supporting Information or can be retrieved from the Cambridge Structural Database (CSD) (CCDC number 1983494).

Table 2. Crystal Data and Structure Refinement Parameters for VLF and VLF−CA

	VLF	VLF−CA
empirical formula	$C_{17}H_{28}NO_2$	$(C_{17}H_{29}NO_2)^+\cdot(C_9H_7O_4)^-$
molecular weight	277.39	457.55
wavelength (Å), CuKα	1.54187	1.54187
description	block	Plate
crystal system	monoclinic	Monoclinic
space group	$P2_1/n$	$P2_1/n$
a (Å)	8.414(1)	13.3663(2)
b (Å)	8.867(1)	13.3663(2)
c (Å)	21.790(3)	17.0804(3)
β (deg)	92.31(1)	102.72(1)
volume (Å^3), Z	1624.2(4), 4	2405.33(7), 4
density (g cm^{-3})	1.134	1.263
F (000)	608	984
θrange/deg	$4.06 \le \theta \le 67.49$	$3.817 \le \theta \le 66.857$
uniq. data, obser data, R_{int}	2884, 2585, 0.0234	4264, 3609, 0.0278
data/restraints/parameters	2884/182/0	4264/304/0
R indices, goodness-of-fit	0.0415, 0.1118, 1.045	0.0451, 0.1161, 1.039
CCDC number	[a]	1983494

[a]Consistent with CCDC refcode OCALAG02.[38]

2.2. Powder X-ray Diffraction. The PXRD is a fast and reliable technique to evaluate the homogeneity and phase purity of the simulated PXRD patterns and the experimental powder patterns.[39] Besides, it is a reliable method to distinguish the multicomponent solid products from their starting materials. Figure 4 shows the PXRD patterns of VLF, CA, and VLF−CA. The VLF showed reflections at 2θ values of 8.18, 11.18, 16.98, 23.85, and 26.22°. The CA showed diffraction peaks at 2θ values of 14.18, 15.88, 17.50, 24.48, 27.10, 30.12, and 33.56°. These diffraction peaks are attributed to the crystalline nature of the starting materials. The physical mixture exhibited a superimposition of the reflections of the individual raw materials of VLF and CA. The experimental powders of VLF−CA salt showed characteristic peaks at 2θ values of 9.47, 13.42, 15.26, 17.88, 18.10, 19.00, 19.56, 19.92, 21.26, 22.02, 22.50, and 22.92°, that are not present in either VLF or CA and which could be attributed to the interactions between the two components, and at the same time, signifies that VLF reacted completely with CA. The purity and homogeneity of each crystalline phase has also been confirmed by comparing the experimental powder patterns with the simulated PXRD patterns calculated from the SXRD data using MERCURY software (Version 2.4; Cambridge Crystallographic Data Center, Cambridge, UK; CCDC refcode OCALAG02 for VLF, FESNOG for CA, and CCDC number 1983494 for VLF−CA).[38,40]

2.3. Thermal Analysis. DSC has unique advantages in terms of its simplicity, rapidity, and ease of measurement providing direct information pertaining to the thermodynamic and kinetic properties associated with solid materials.[41] DSC is a prime technique to validate the purity of the material and understand phase transformations. Figure 5a shows the DSC thermograms of VLF−CA salt, VLF, CA, and their physical mixture. The sharp endothermic peak of VLF−CA at 149.02 °C was different from the peaks of VLF (79.18 °C) and CA (221.72 °C), besides, the physical mixture of VLF and CA showed endothermic peaks at 76.17 and 135.88 °C, which collaboratively confirmed the creation of the new solid phase. The higher endothermic peak of the VLF−CA salt also hints at a higher thermodynamic stability.

The TGA pattern is shown in Figure 5b. There is no evidence of weight loss of either the solvent or water, indicating that the sample was anhydrous and solvent-free, and in accordance with the observed SXRD data.

2.4. ^{13}C Solid-State Nuclear Magnetic Resonance Measurement. The ssNMR is an another often employed technique for the analysis of solid forms of pharmaceuticals.[42] The ^{13}C CP/MAS TOSS NMR spectra of venlafaxine salt and their starting materials are shown in Figure 6. Upon the salt formation, the chemical shift of the carboxylic signal was altered from 175.7 to 174.7 ppm, and the signal of the N bonded C site altered from 62.7 to 59.1 ppm, whose shielding effect was enhanced by the proton transfer. These shifts can be used as supporting evidence of the salt formation.

https://doi.org/10.1021/acsomega.1c01581
ACS Omega 2021, 6, 13895−13903

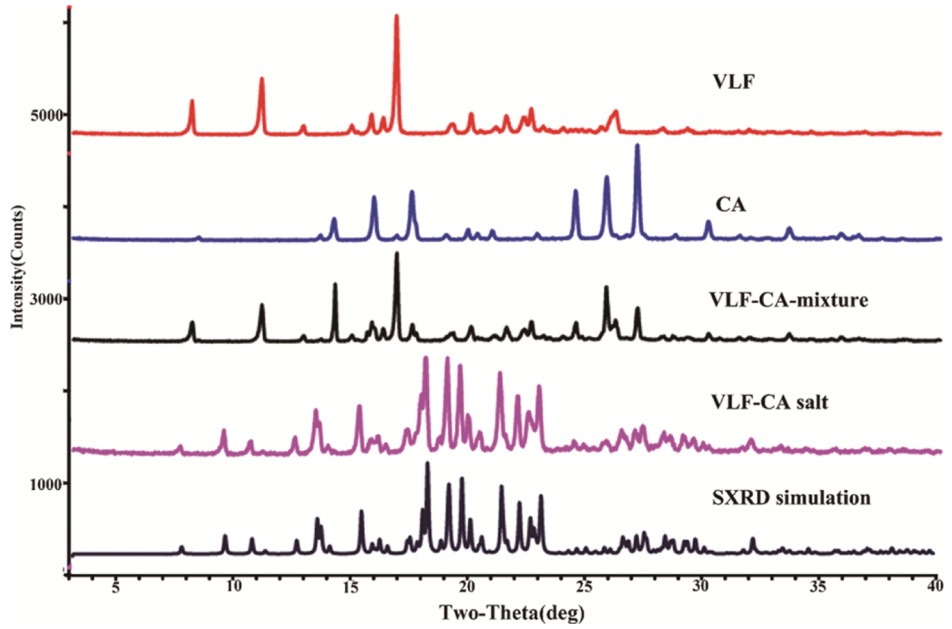

Figure 4. PXRD patterns of VLF−CA and the raw materials.

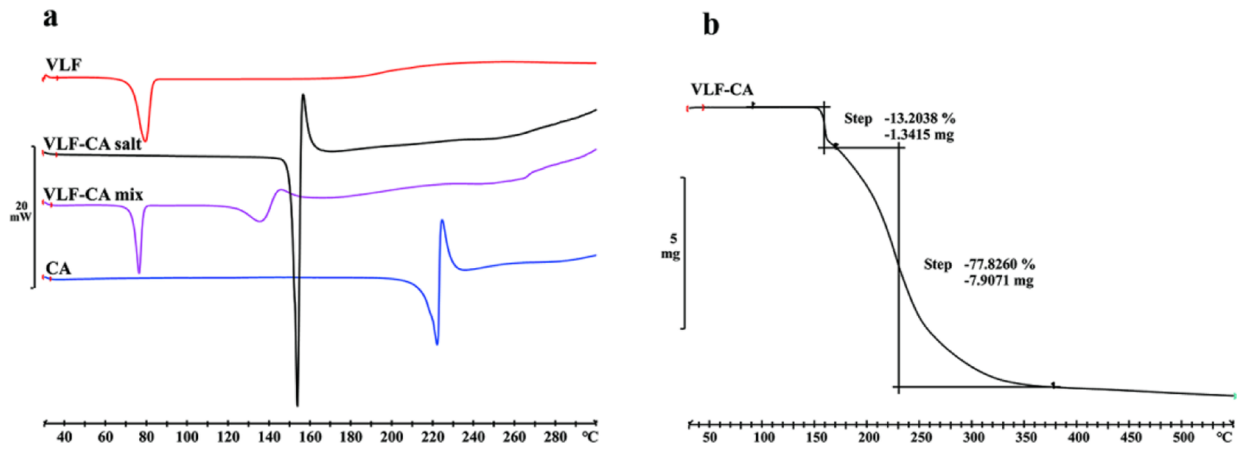

Figure 5. DSC thermograms of VLF−CA, the raw materials, and physical mixture (a), and the TGA pattern of VLF−CA (b).

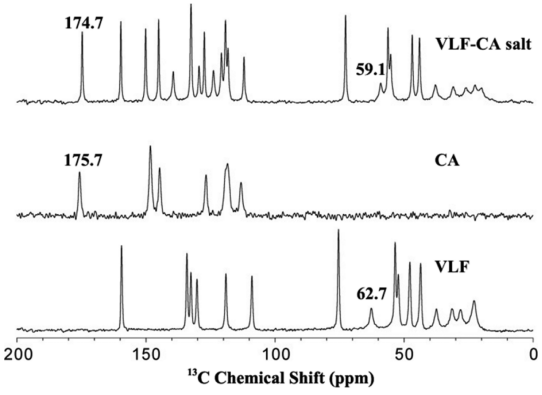

Figure 6. ^{13}C NMR spectra of VLF−CA and the raw materials.

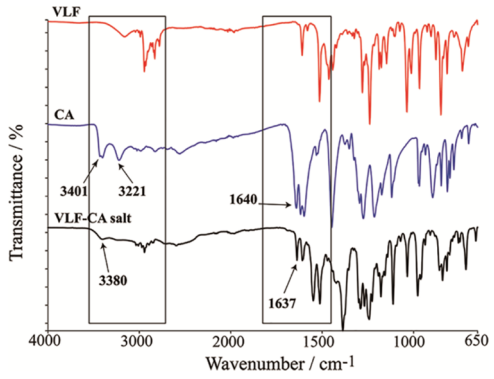

Figure 7. FT-IR spectra of VLF−CA and the raw materials.

2.5. FT-IR Spectroscopy. FT-IR spectroscopy study was performed to identify the noncovalent interactions within the crystal.[43] A shift in the carbonyl group of the acid or amide derivatives is common when the group is involved in intermolecular interactions. Figure 7 shows the IR spectra of VLF, CA, and VLF−CA. In the present study, the stretching vibration of −COOH group of CA observed at 3401 cm^{-1} disappeared in VLF−CA, indicating that deprotonation has occurred on the −OH group of CA. The C═O group of CA was observed at 1640 cm^{-1} (S), while there is a weaker absorption peak at 1637 cm^{-1} in VLF−CA salt, which could be

https://doi.org/10.1021/acsomega.1c01581
ACS Omega 2021, 6, 13895−13903

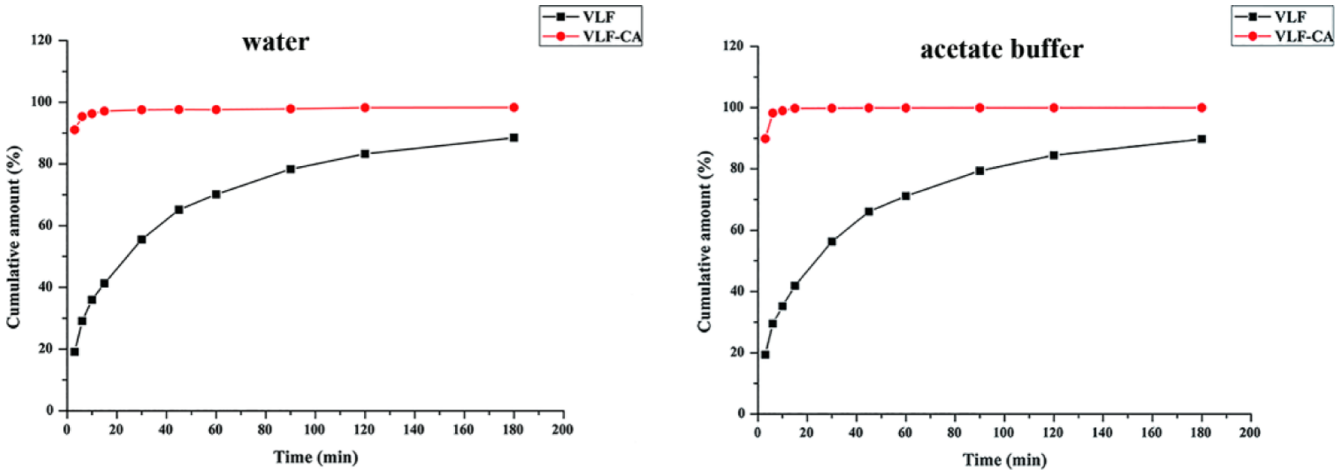

Figure 8. Dissolution studies of VLF and VLF−CA in distilled water and acetate buffer.

Table 3. VLF−CA Hypoglycemic Activity *in Vitro*[a]

	DMSO	VLF−CA 125 μM	VLF−CA 250 μM	VLF−CA 500 μM	Met 5 mM
glucose consumption level (mM)	2.13 ± 0.08	2.28 ± 0.22	3.30 ± 0.67**	3.68 ± 0.52***	3.38 ± 0.25***
glucose consumption index	1.00	1.07	1.54	1.73	1.59

[a]*p < 0.05, **p < 0.01, ***p < 0.001 versus DMSO.

attributed to the restriction from −NH of VLF. The −OH group of CA observed at 3221 cm^{-1} disappeared in VLF−CA, resulting from the intermolecular hydrogen bonds of O_5−H_{5A}···O_4 and O_6−H_{6A}···O_3. Besides, there is an absorption peak at 3380 cm^{-1} in VLF−CA, which belongs to the $-NR_3H^+$ of VLF−CA. Unambiguously, IR spectra comparisons of the synthesized salt and the individual starting materials help to construe the salt formation.

2.6. Stability Study. The chemical stability of pharmaceutical products is of great importance due to its intrinsic effects on the safety and efficacy of drug molecules. The FDA and ICH guidelines clearly state the requirements of stability testing data to understand the quality of the drug substance changing with time under the influence of various environmental factors. In the present study, to investigate the potential physical stability concerns, a long-term stability study was monitored at a temperature of 25 ± 2 °C and the relative humidity maintained at 60 ± 5% for 12 months. Consequently, the phase purity of the material was determined by the PXRD technique by comparing the diffraction patterns of the initial and final samples (Supporting Information Figure S4). The results of PXRD measurements demonstrated that the PXRD patterns of VLF−CA salt did not change, indicating a stable solid phase for 12 months at 25 °C/60% RH.

2.7. Solubility and Dissolution. One of the main purposes of this work is to improve the solubility of the poorly water-soluble VLF by employing salt formation. In the case of pure VLF, the maximum concentration is 0.39 mg mL^{-1}, while for VLF−CA, the maximum concentration reached 6.28 mg mL^{-1} in distilled water. It can be clearly seen, by virtue of interactions with the acidic coformer CA, that the solubility of VLF in the salt form is enhanced significantly with a 16-fold solubility increase obtained in VLF−CA as compared to that of the parent drug. Moreover, the VLF−CA salt possesses a faster dissolution rate than VLF in distilled water (pH = 7.0) and acetate buffer (pH = 4.5) in powder dissolution measurements (Figure 8), suggesting a potential for increasing the absorption and hence, the bioavailability of VLF.[44−46]

The dissolution profiles of VLF and VLF−CA in HCl solution (pH = 1.2) and phosphate buffer (pH = 6.8) were also evaluated, and there appears to be no distinction between VLF and VLF−CA with the release of VLF being completed within 20 min (Figure S5).

2.8. Glucose Consumption Assay. To determine the effects of VLF−CA on the cellular glucose consumption, human liver cells of HL-7702 were treated with VLF−CA for 12 h, and Metformin (Met) was used as the positive control. As shown in Table 3, VLF−CA stimulated glucose consumption at 125, 250, and 500 μM dose-dependently in HL-7702. Especially, VLF−CA at 250 μM caused a significant increase in the glucose consumption (p < 0.01 vs DMSO), with the glucose consumption level and index reaching 3.30 ± 0.67 mM and 1.54, respectively, and its efficacy was comparable to that of 5 mM metformin, whose glucose consumption index was 1.59. Moreover, when the concentration of VLF−CA reached 500 μM, the glucose consumption activity was more potent than that of metformin at 5 mM, and the glucose consumption level and index reached 3.68 ± 0.52 mM and 1.73, respectively. The results showed that VLF−CA possesses potent hypoglycemic activity *in vitro*.

3. CONCLUSIONS

A new ionic salt composed of venlafaxine and caffeic acid in a 1:1 molecular ratio was successfully synthesized for the first time. The crystal structure confirmed the proton transfer from the carboxyl group of the coformer CA to the amino group in VLF. The three-dimensional hydrogen-bonded networks constructed contact with salt-bond and hydrogen-bond interactions. Besides, the characterizations by the combined techniques of PXRD, DSC, TGA, FT-IR, and ssNMR consistently provide strong identifications of the creation of the new solid form.

https://doi.org/10.1021/acsomega.1c01581
ACS Omega 2021, 6, 13895−13903

A 16-fold higher solubility, improved dissolution behavior than the corresponding starting compound VLF, and excellent long-term stability imply that the VLF−CA salt can be selected for further development. It is worth noting that the solubility of the active component can be substantially increased when the salt formation technology is employed, as demonstrated in the present study.

The literature shows that there is a high prevalence of depression and diabetes distress, giving us the inspiration for developing novel candidates effective for patients with major depression disorder and diabetes. At the same time, the glucose consumption assay, inspired by hypoglycemic symptoms following venlafaxine intoxication, showed that VLF−CA possesses potent hypoglycemic activity *in vitro*. Although further experimental studies regarding the investigation of the hypoglycemic mechanism of VLF−CA with *in vivo* pharmacokinetic data are required, it can be suggested that the new salt may be developed as a promising candidate for the next stage of treatment for major depressive disorder patients with type 2 diabetes.

This work indicated that the introduction of a coformer could certainly alter some physicochemical and biomedical properties of an active pharmaceutical ingredient (API), which could be either the melting point, stability, solubility, dissolution rate, or pharmacological activity. Notably, a new indication of controlling the sugar level by VLF−CA salt was discovered in the study, which deserves an in-depth research.

4. MATERIALS AND METHODS

4.1. Materials and Reagents. Venlafaxine hydrochloride raw material was purchased from Wuhan Yinhe Chemical Co., Ltd. (Hubei, China). Caffeic acid (CA) was purchased from Chengdu Must Biotechnology Co., Ltd. (Sichuan, China). All chemicals (reagent quality) were obtained from commercial sources and used without further purification. Human liver cells of HL-7702 were purchased from the Institute of Biochemistry and Cell Biology Sciences, Chinese Academy of Sciences (Shanghai, China). RPMI 1640 medium, fetal bovine serum, and trypsin were purchased from Gibco-Invitrogen (Grand Island, NY, USA). Glucose Assay Kit (based on glucose oxidase method) was purchased from Beijing Strong Biotechnologies, Inc. (Beijing, China).

4.2. Preparation of Compounds. VLF was prepared as per the procedure described in the literature.[47] VLF−CA was obtained by three different methods including crystallization, liquid-assisted grinding, and slurry methods. The suitable crystal was collected and used for the single-crystal diffraction analysis. The details of VLF and VLF−CA preparations are described in the Supporting Information.

4.3. X-ray Diffraction Analysis. A Rigaku Micromax 002+ diffractometer (USA), with a CCD detector and a graphite monochromator (CuKa radiation, λ = 1.54187 Å), was used to record the SXRD data of VLF salt with CA as a coformer. Data collections were performed at 295 K using a CrysAlisPro system attached to the diffractometer. The collection, reduction, and absorption corrections were carried out using CrystalClear (Rigaku Inc., 2008). All structures were solved by SHELXS-2016 (Sheldrick, 2016) using a direct method and refined by SHELXL-2016 (Sheldrick, 2016) using a full-matrix least-squares technique. Anisotropic displacement parameters were applied for refinements of non-hydrogen atoms, and hydrogen atoms were either placed in their calculated positions or located from the difference in the electron density map, refined as riding atoms using isotropic displacement parameters. Analyses of SXRD data were carried out using the OLEX2 program, and MERCURY software (Version 2.4) was employed to prepare molecular diagrams.

A Rigaku D/max-2550 (Japan) instrument was used for the PXRD data collection of the salt and the raw materials. Monochromatic CuKa radiation was used as a source with wavelength λ = 1.54178 Å. The tube voltage and current were set at 45 kV and 150 mA, respectively. The samples were scanned over a 2θ range from 3 to 40° with a step size of 0.02° and a scan speed of 8 °C/min. The instrument was calibrated using an Al_2O_3 standard material before the experiments. The analyses of the patterns were performed using Jade 6.0 software and the images were generated by the Adobe Illustrator CS5 program.

4.4. Thermal Analysis. DSC analyses were conducted on a Mettler−Toledo DSC1 instrument. The accurately weighed (4 mg) samples in hermetically sealed aluminum crucibles (40 μL) with a pinhole were heated from 30 to 300 °C at a constant rate of 10 °C min^{-1}.

The TGA measurement was performed on a Mettler−Toledo TGA/DSC apparatus. The accurately weighed (10 mg) samples in aluminum oxide crucibles were heated from 30 to 550 °C at a constant ramp of 10 °C min^{-1} under a stream of dry nitrogen gas flow at 50 mL min^{-1}. The STARe software was employed to record and analyze the TGA/DSC data.

4.5. FT-IR Spectroscopy. FT-IR spectra were recorded using a PerkinElmer Spectrum 400 FT-IR instrument, equipped with attenuated total reflectance with a diamond crystal. For all the analyses, background data collection was performed before sample measurements. All spectra were acquired in the range of 650−4000 cm^{-1} with 16 scans at a resolution of 4 cm^{-1}.

4.6. Solid-State NMR Measurements. A Bruker AVANCE III-500 spectrometer equipped with a 4 mm double resonance MAS probe was used to perform the solid-state NMR measurements. A total sideband suppression frame was embedded in the standard CP pulse program to remove the spinning sidebands. An 8 kHz MAS spinning frequency with a 2 ms contact time was used in the ^{13}C ssNMR experiments. The recycle delay parameters were set at 30 s for CA and 8 s for VLF and VLF−CA.

4.7. Solubility Determination and Dissolution Analysis. The comparative solubility study of the VLF and VLF−CA was conducted using the saturation shake-flask method. The samples of VLF and VLF−CA were milled in an agate mortar to homogenize the particle size and thereby avoid particle size effects. About 100 mg of the samples were added into a conical flask containing distilled water (10 mL), and then, the resulting solutions were placed in a ZHWY-103D thermostatic shaker-incubator (Shanghai Zhicheng Analytical Instrument Manufacturing Co., Ltd.). The solutions were kept at 37 ± 0.5 °C and agitated continuously at a rate of 150 strokes min^{-1} for 48 h, and subsequently, 1 mL of the sample solutions were withdrawn through 0.22 μm nylon filters. Subsequently, after appropriate dilution, 5 μL of the solutions were injected into an Agilent 1260 high-performance liquid chromatography (HPLC) system to quantify the concentration of VLF. The chromatography conditions were as follows: a Linksil-ODS 5 μm (150 mm × 4.6 mm) column; the mobile phase, acetonitrile, and 0.1 mol L^{-1} potassium dihydrogen phosphate water solution (32/68, *v*/*v*); flow rate, 1.0 mL

https://doi.org/10.1021/acsomega.1c01581
ACS Omega 2021, 6, 13895−13903

min^{-1}; column temperature, 35 °C; injection volume, 5 μL; and detection wavelength, 225 nm.

The dissolution analyses of VLF−CA and VLF were carried out at a constant temperature of 37 °C using a ZHWY-103D constant temperature shaking-incubator (Shanghai Zhicheng Analytical Instrument Manufacturing Co., Ltd.), and the concentration of VLF was measured by Agilent 1260 HPLC instrument. Powder equivalents of 5.00 mg of VLF were added to 75 mL of the dissolution medium of distilled water (pH 7.0) and acetate buffer solution (pH 4.5). The solution was kept homogeneous by continuous shaking at 160 strokes min^{-1}. At regular time-intervals of 3, 6, 10, 15, 30, 45, 60, 90, 120, and 180 min, 5 mL of the dissolution medium was withdrawn and replaced by an equal volume of fresh medium to maintain a constant volume. The samples were filtered through 0.22 μm nylon filters for drug content assay. The filtrates, after appropriate dilution, were determined using the HPLC method.

The HPLC method development and validation parameters are provided in the Supporting Information.

4.8. HL-7702 Culture and Characterization. The HL-7702 cells were cultured in 96-well plates and treated with either DMSO or VLF−CA (125, 250, and 500 μM) or 5 mM of metformin at 37 °C and 5% CO_2 for 12 h. After the treatment for the indicated duration, the supernatant was taken for glucose detection. The glucose consumption index was used to evaluate drug hypoglycemic activity *in vitro*.

■ ASSOCIATED CONTENT

Supporting Information

The Supporting Information is available free of charge at https://pubs.acs.org/doi/10.1021/acsomega.1c01581.

Supporting Information related to this article can be found in the supplementary files.(pdf/cif) HPLC method development and validation parameters, preparation methods of VLF starting materials, and VLF−CA salt powders, standard curve of VLF−CA sample solution, HPLC patterns of VLF−CA and raw materials, ORTEP-type view of the asymmetric unit with 50% probability ellipsoid, PXRD patterns of VLF−CA before and after the long-term stability test, and dissolution profiles of VLF and VLF−CA in hydrochloric acid solution (PH = 1.2) and phosphate buffer (PH = 6.8)(PDF)

X-ray crystallographic data (CIF)

Accession Codes

CCDC 1983494 contains the supplementary crystallographic data of VLF−CA.

■ AUTHOR INFORMATION

Corresponding Authors

Ningbo Gong − *Beijing Key Laboratory of Polymorphic Drugs, Institute of Materia Medica, Chinese Academy of Medical Sciences and Peking Union Medical College, Beijing 100050, China*; Phone: +86 01063030566; Email: gnb@imm.ac.cn

Yang Lu − *Beijing Key Laboratory of Polymorphic Drugs, Institute of Materia Medica, Chinese Academy of Medical Sciences and Peking Union Medical College, Beijing 100050, China*; orcid.org/0000-0002-2274-5703; Phone: +86 01063165212; Email: luy@imm.ac.cn; Fax: +86 01063165212

Authors

Hongmei Yu − *Beijing Key Laboratory of Polymorphic Drugs, Institute of Materia Medica, Chinese Academy of Medical Sciences and Peking Union Medical College, Beijing 100050, China*; orcid.org/0000-0002-8279-7513

Yong Zhang − *Hainan Medical University, Haikou 571199, China*

Cheng Xing − *Beijing Key Laboratory of Polymorphic Drugs, Institute of Materia Medica, Chinese Academy of Medical Sciences and Peking Union Medical College, Beijing 100050, China*

Ying Wang − *Beijing Key Laboratory of Polymorphic Drugs, Institute of Materia Medica, Chinese Academy of Medical Sciences and Peking Union Medical College, Beijing 100050, China*

Hailu Zhang − *Laboratory of Magnetic Resonance Spectroscopy and Imaging, Suzhou Institute of Nano-Tech and Nano-Bionics, Chinese Academy of Sciences, Suzhou 215123, China*

Guanhua Du − *Beijing City Key Laboratory of Drug Target Identification and Drug Screening, Institute of Materia Medica, Chinese Academy of Medical Sciences and Peking Union Medical College, Beijing 100050, China*

Complete contact information is available at: https://pubs.acs.org/10.1021/acsomega.1c01581

Author Contributions

H.Y. prepared the samples, analyzed and wrote the original draft; Y.Z. performed the pharmacological study; C.X., Y.W., and H.Z. performed the spectroscopy measurements of the samples; N.G. performed the crystal analysis, revised and approved the manuscript; Y.L. and G.D. revised and approved the manuscript.

Notes

The authors declare no competing financial interest.

■ ACKNOWLEDGMENTS

We thank CAMS Innovation Fund for Medical Sciences (no.2017-I2M-1-010, 2020-I2M-1-003), National Key Research and Development Programmes (no.2016YFC1000901), Construction and Application of Technology Integration System for Efficient Identification of Natural/Effective Active Small Molecules (no. 2018ZX09711001-001), and the National Natural Science Foundation of China (no. 21874148) for the financial support.

■ REFERENCES

(1) Shea, M. L. O.; Garfield, L. D.; Teitelbaum, S.; Civitelli, R.; Mulsant, B. H.; Reynolds, C. F.; Dixon, D.; Doré, P.; Lenze, E. J. Serotonin-norepinephrine reuptake inhibitor therapy in late-life depression is associated with increased marker of bone resorption. *Osteoporos. Int.* **2013**, *24*, 1741−1749.

(2) Gutierrez, M. A.; Stimmel, G. L.; Aiso, J. Y. Venlafaxine: a 2003 update. *Clin. Ther.* **2003**, *25*, 2138−2154.

(3) Tian, Y.; Du, J.; Spagna, A.; Mackie, M.-A.; Gu, X.; Dong, Y.; Fan, J.; Wang, K. Venlafaxine treatment reduces the deficit of executive control of attention in patients with major depressive disorder. *Sci. Rep.* **2016**, *6*, 28028.

(4) Marlow, N. M.; Simpson, K. N.; Vaughn, I. A.; Jo, A.; Zoller, J. S.; Short, E. B. Healthcare Costs and medication adherence among patients with fibromyalgia: combination medication vs. duloxetine, milnacipran, venlafaxine, and pregabalin initiators. *Pain Pract.* **2018**, *18*, 154−169.

(5) Cohen, L. S.; Viguera, A. C.; Bouffard, S. M.; Nonacs, R. M.; Morabito, C.; Collins, M. H.; Ablon, J. S. Venlafaxine in the treatment of postpartum depression. *J. Clin. Psychiatr.* **2001**, *62*, 592.
(6) Denys, D.; van der Wee, N.; van Megen, H. J. G. M.; Westenberg, H. G. M. A double blind comparison of venlafaxine and paroxetine in obsessive-compulsive disorder. *J. Clin. Psychopharmacol.* **2003**, *23*, 568−575.
(7) Li, X.; Zhu, L.; Su, Y.; Fang, S. Short-term efficacy and tolerability of venlafaxine extended release in adults with generalized anxiety disorder without depression: A meta-analysis. *PloS One* **2017**, *12*, No. e0185865.
(8) Aiyer, R.; Barkin, R. L.; Bhatia, A. Treatment of neuropathic pain with venlafaxine: a systematic review. *Pain Med.* **2017**, *18*, 1999−2012.
(9) Trouvin, A.-P.; Perrot, S.; Lloret-Linares, C. Efficacy of venlafaxine in neuropathic pain: a narrative review of optimized treatment. *Clin. Ther.* **2017**, *39*, 1104−1122.
(10) Ghanizadeh, A.; D. Freeman, R.; Berk, M. Efficacy and adverse effects of venlafaxine in children and adolescents with ADHD: a systematic review of non-controlled and controlled trials. *Rev. Recent Clin. Trials* **2013**, *8*, 2−8.
(11) Farshchian, N.; Alavi, A.; Heydarheydari, S.; Moradian, N. Comparative study of the effects of venlafaxine and duloxetine on chemotherapy-induced peripheral neuropathy. *Canc. Chemother. Pharmacol.* **2018**, *82*, 787−793.
(12) Holliday, S. M.; Benfield, P. Venlafaxine. *Drugs* **1995**, *49*, 280−294.
(13) Roy, S.; Aitipamula, S.; Nangia, A. Thermochemical analysis of venlafaxine hydrochloride polymorphs 1−5. *Cryst. Growth Des.* **2005**, *5*, 2268−2276.
(14) Van Eupen, J. T. H.; Elffrink, W. W. J.; Keltjens, R.; Bennema, P.; De Gelder, R.; Smits, J. M. M.; van Eck, E. R. H.; Kentgens, A. P. M.; Deij, M. A.; Meekes, H.; Vlieg, E. Polymorphism and migratory chiral resolution of the free base of venlafaxine. A remarkable topotactical solid state transition from a racemate to a racemic conglomerate. *Cryst. Growth Des.* **2008**, *8*, 71−79.
(15) Roy, S.; Bhatt, P. M.; Nangia, A.; Kruger, G. J. Stable polymorph of venlafaxine hydrochloride by solid-to-solid phase transition at high temperature. *Cryst. Growth Des.* **2007**, *7*, 476−480.
(16) Vega, D.; Fernández, D.; Echeverría, G. 1-[2-(1-Hydroxycyclohexyl)-2-(4-methoxyphenyl) ethyl] dimethylammonium chloride (venlafaxine hydrochloride). *Acta Crystallogr., Sect. C: Cryst. Struct. Commun.* **2000**, *56*, 1009−1010.
(17) Yardley, J. P.; Husbands, G. E. M.; Stack, G.; Butch, J.; Bicksler, J.; Moyer, J. A.; Muth, E. A.; Andree, T.; Fletcher, H., III 2-Phenyl-2-(1-hydroxycycloalkyl)ethylamine derivatives: synthesis and antidepressant activity. *J. Med. Chem.* **1990**, *33*, 2899−2905.
(18) Spinelli, F.; Dichiarante, E.; Curzi, M.; Giaffreda, S. L.; Chierotti, M. R.; Gobetto, R.; Rossi, F.; Chelazzi, L.; Braga, D.; Grepioni, F. Molecular salts of the antidepressant venlafaxine: an effective route to solubility properties modifications. *Cryst. Growth Des.* **2017**, *17*, 4270−4279.
(19) Gong, N.; Zhang, Y.; Wang, Y.; Yu, H.; Zhang, B.; Zhang, H.; Lu, Y.; Du, G. Versatile Salts as a Strategy to Modify the Biopharmaceutical Properties of Venlafaxine and a Potential Hypoglycemic Effect Study. *Cryst. Growth Des.* **2020**, *20*, 3131−3139.
(20) Srivastava, D.; Fatima, Z.; Kaur, C. D. Multicomponent Pharmaceutical Cocrystals: A Novel Approach for Combination Therapy. *Mini-Rev. Med. Chem.* **2018**, *18*, 1160−1167.
(21) Aldhyani, T. H. H.; Alshebami, A. S.; Alzahrani, M. Y. Soft clustering for enhancing the diagnosis of chronic diseases over machine learning algorithms. *J. Healthc. Eng.* **2020**, *2020*, 4984967.
(22) Réus, G. Z.; dos Santos, M. A. B.; Strassi, A. P.; Abelaira, H. M.; Ceretta, L. B.; Quevedo, J. Pathophysiological mechanisms involved in the relationship between diabetes and major depressive disorder. *Life Sci.* **2017**, *183*, 78−82.
(23) Afghahi, H.; Svensson, M. K.; Pirouzifard, M.; Eliasson, B.; Svensson, A.-M. Blood pressure level and risk of major cardiovascular events and all-cause of mortality in patients with type 2 diabetes and renal impairment: an observational study from the swedish national diabetes register. *Diabetologia* **2015**, *58*, 1203−1211.
(24) Lustman, P. J.; Anderson, R. J.; Freedland, K. E.; De Groot, M.; Carney, R. M.; Clouse, R. E. Depression and poor glycemic control: a meta-analytic review of the literature. *Diabetes Care* **2000**, *23*, 934−942.
(25) De Groot, M.; Anderson, R.; Freedland, K. E.; Clouse, R. E.; Lustman, P. J. Association of depression and diabetes complications: a meta-analysis. *Psychosom. Med.* **2001**, *63*, 619−630.
(26) Zhang, Y.; Ting, R. Z.; Yang, W.; Jia, W.; Li, W.; Ji, L.; Guo, X.; Kong, A. P.; Wing, Y. K.; Luk, A. O.; Sartorius, N.; Morisky, D. E.; Oldenburg, B.; Weng, J.; Chan, J. C. Depression in C hinese patients with type 2 diabetes: associations with hyperglycemia, hypoglycemia, and poor treatment adherence. *J. Diabetes* **2015**, *7*, 800−808.
(27) Rustad, J. K.; Musselman, D. L.; Nemeroff, C. B. The relationship of depression and diabetes: pathophysiological and treatment implications. *Psychoneuroendocrinology* **2011**, *36*, 1276−1286.
(28) Musselman, D. L.; Betan, E.; Larsen, H.; Phillips, L. S. Relationship of depression to diabetes types 1 and 2: epidemiology, biology, and treatment. *Biol. Psychiatry* **2003**, *54*, 317−329.
(29) Fisher, L.; Skaff, M. M.; Mullan, J. T.; Arean, P.; Glasgow, R.; Masharani, U. A longitudinal study of affective and anxiety disorders, depressive affect and diabetes distress in adults with type 2 diabetes. *Diabetic Med.* **2008**, *25*, 1096−1101.
(30) Fisher, L.; Gonzalez, J. S.; Polonsky, W. H. The confusing tale of depression and distress in patients with diabetes: a call for greater clarity and precision. *Diabetic Med.* **2014**, *31*, 764−772.
(31) Kreider, K. E. Diabetes distress or major depressive disorder? A practical approach to diagnosing and treating psychological comorbidities of diabetes. *Diabetes Ther.* **2017**, *8*, 1−7.
(32) Mezuk, B.; Eaton, W. W.; Albrecht, S.; Golden, S. H. Depression and Type 2 Diabetes Over the Lifespan: A meta-analysis. *Diabetes Care* **2008**, *31*, 2383−2390.
(33) Cyuńczyk, A.; Misiak, B.; Lewko, K.; Dziekońska, M.; Lewko, J. Relationship between sociodemographic factors and depression symptoms and level of diabetes acceptance. *Prog. Health Sci.* **2019**, *2*, 21−28.
(34) Talbot, F.; Nouwen, A. A review of the relationship between depression and diabetes in adults: is there a link? *Diabetes Care* **2000**, *23*, 1556−1562.
(35) Ling, Y.; Khara, L.; Alvarez, G.; McBeth, P. B. Persistent Hypoglycemia in Venlafaxine Overdose. *Arch. Clin. Med. Case Rep.* **2019**, *03*, 94−99.
(36) Brvar, M.; Koželj, G.; Mašič, L. P. Hypoglycemia in venlafaxine overdose: a hypothesis of increased glucose uptake. *Eur. J. Clin. Pharmacol.* **2015**, *71*, 261−262.
(37) Vioglio, P. C.; Chierotti, M. R.; Gobetto, R. Pharmaceutical aspects of salt and cocrystal forms of APIs and characterization challenges. *Adv. Drug Delivery Rev.* **2017**, *117*, 86−110.
(38) van Eupen, J. T. H.; Elffrink, W. W. J.; Keltjens, R.; Bennema, P.; de Gelder, R.; Smits, J. M. M.; van Eck, E. R. H.; Kentgens, A. P. M.; Deij, M. A.; Meekes, H.; Vlieg, E. Polymorphism and migratory chiral resolution of the free base of venlafaxine. A remarkable topotactical solid state transition from a racemate to a racemic conglomerate. *Cryst. Growth Des.* **2008**, *8*, 71−79.
(39) Thakral, N. K.; Zanon, R. L.; Kelly, R. C.; Thakral, S. Applications of powder X-ray diffraction in small molecule pharmaceuticals: Achievements and aspirations. *J. Pharm. Sci.* **2018**, *107*, 2969−2982.
(40) García-Granda, S.; Beurskens, G.; Beurskens, P. T.; Krishna, T. S. R.; Desiraju, G. R. Structure of 3,4-dihydroxy-trans-cinnamic acid (caffeic acid) and its lack of solid-state topochemical reactivity. *Acta Crystallogr., Sect. C: Cryst. Struct. Commun.* **1987**, *43*, 683−685.
(41) Korhammer, K.; Neumann, K.; Opel, O.; Ruck, W. K. L. Thermodynamic and kinetic study of $CaCl_2$-CH_3OH adducts for solid sorption refrigeration by TGA/DSC. *Appl. Energy* **2018**, *230*, 1255−1278.

https://doi.org/10.1021/acsomega.1c01581
ACS Omega 2021, 6, 13895−13903

(42) Martins, I. C. B.; Sardo, M.; Alig, E.; Fink, L.; Schmidt, M. U.; Mafra, L.; Duarte, M. T. Enhancing adamantylamine solubility through salt formation: novel products studied by X-ray diffraction and solid-state NMR. *Cryst. Growth Des.* **2019**, *19*, 1860−1873.
(43) Pandey, N. K.; Sehal, H. R.; Garg, V.; Gaur, T.; Kumar, B.; Singh, S. K.; Gulati, M.; Gowthamarajan, K.; Bawa, P.; Rajesh, S. Y.; et al. Stable co-crystals of glipizide with enhanced dissolution profiles: preparation and characterization. *AAPS PharmSciTech* **2017**, *18*, 2454−2465.
(44) Dokoumetzidis, A.; Macheras, P. A century of dissolution research: from noyes and whitney to the biopharmaceutics classification system. *Int. J. Pharm.* **2006**, *321*, 1−11.
(45) Beveridge, T.; Schmidt, R.; KalbererNüesch, F. E. Bioavailability of digoxin. *Lancet* **1972**, *2*, 592.
(46) Chapron, D. J.; Kramer, P. A.; Mariano, S. L.; Hohnadel, D. C. Effect of calcium and antacids on phenytoin bioavailability. *Arch. Neurol.* **1979**, *36*, 436−438.
(47) Liu, Z.-J.; Liu, H.; Chen, X. W.; Lin, M.; Hu, Y.; Tuo, X.; Yuan, Z. Y.; Sun, X. X. Efficient resolution of venlafaxine and mechanism study via X-ray crystallography. *Chirality* **2017**, *30*, 268−274.

https://doi.org/10.1021/acsomega.1c01581
ACS Omega 2021, 6, 13895−13903